Draft version February 24, 2016
Preprint typeset using LaTeX style emulateapj v. 5/2/11

arXiv:1602.07244v1 [astro-ph.SR] 23 Feb 2016

THE NONPOTENTIALITY OF CORONAE OF SOLAR ACTIVE REGIONS, THE DYNAMICS OF THE SURFACE MAGNETIC FIELD, AND THE POTENTIAL FOR LARGE FLARES

Carolus J. Schrijver
Lockheed Martin Advanced Technology Center (A021S, Bldg. 252),
3251 Hanover Street, Palo Alto, CA 94304

Draft version February 24, 2016

ABSTRACT

Flares and eruptions from solar active regions are associated with atmospheric electrical currents accompanying distortions of the coronal field away from a lowest-energy potential state. In order to better understand the origin of these currents and their role in M- and X-class flares, I review all active-region observations made with *SDO/HMI* and *SDO/AIA* from 2010/05 through 2014/10 within $\approx 40^\circ$ from disk center. I select the roughly 4% of all regions that display a distinctly nonpotential coronal configuration in loops with a length comparable to the scale of the active region, and all that emit GOES X-class flares. The data for 41 regions confirm, with a single exception, that strong-field, high-gradient polarity inversion lines (SHILs) created during emergence of magnetic flux into, and related displacement within, pre-existing active regions are associated with X-class flares. Obvious nonpotentiality in the active region-scale loops occurs in 6 of 10 selected regions with X-class flares, all with relatively long SHILs along their primary polarity inversion line, or with a long internal filament there. Nonpotentiality can exist in active regions well past the flux-emergence phase, often with reduced or absent flaring. I conclude that the dynamics of the flux involved in the compact SHILs is of preeminent importance for the large-flare potential of active regions within the next day, but that their associated currents may not reveal themselves in active region-scale nonpotentiality. In contrast, active region-scale nonpotentiality, which can persist for many days, may inform us about the eruption potential other than those from SHILs which is almost never associated with X-class flaring.

Subject headings: Sun: magnetic fields, Sun: flares

1. INTRODUCTION

The "free energy" in the corona over solar active regions that enables flares and eruptions is associated with distortions of the field away from the potential state, quantified through $\nabla \times \mathbf{B}$ and reflected in electrical currents that run through the high atmosphere. Schrijver *et al.* (2005) compared potential-field source-surface (PFSS, specifically using the assimilation-based magnetogram sequence described by Schrijver and DeRosa 2003) extrapolations over a sample of 95 active regions based on magnetograms made with *SOHO's Michelson Doppler Imager* (*MDI*, Scherrer *et al.* 1995) to extreme ultraviolet (EUV) observations of their coronae made with the *Transition Region and Coronal Explorer* (*TRACE*, Handy *et al.* 1999). They concluded that "significant nonpotentiality of the overall active-region coronal field occurs (1) when new flux has emerged within or very near a region within the last $\sim$30 hr, resulting in complex polarity separation lines, or (2) when rapidly evolving, opposite-polarity concentrations are in contact at $4''$ resolution. If these criteria are met by more than 15% of the regions flux, they correctly identify the (non)potentiality of active-region coronae in 88% of the cases."

The nonpotentiality attending these characteristics of the field is clearly correlated with flaring: Schrijver *et al.* (2005), for example, note that C-, M-, and X-class "[f]lares are found to occur 2.4 times more frequently in active regions with nonpotential coronae than in near-potential regions, while their average X-ray peak flare brightness is 3.3 times higher." They further argue "that the currents associated with coronal nonpotentiality have a characteristic growth and decay timescale of $\sim$10-30 hr" and "that shear flows drive enhanced flaring or coronal nonpotentiality only if associated with complex and dynamic flux emergence within the above timescale." Yet, nonpotentiality and flaring appear to be related only in a statistical sense: they find that if "the occurrence of [C-, M-, and X-class] flares in the 3 day window is used as a test for potential and nonpotential coronal fields, only 65% of the regions are correctly identified [...], which is only 15% better than a random selection."

The brightest flares on the GOES scale appear to require quite compact polarity-inversion lines (see the review by Schrijver 2009, and references therein). For example, based on analysis of *MDI* and *TRACE* data on 289 M- and X-class flares, Schrijver (2007) suggested that such flaring was generally connected to flux within some 15 Mm of "pronounced high-gradient polarity-separation lines". The higher the flux included in such regions, the larger the maximum flare peak brightness to be expected, and the larger the probability of such flaring to occur within a given time interval.

Such flare-related strong-field high-gradient inversion lines (referred to as SHILs below) appeared to generally accompany flux emergence, as was confirmed independently by Welsch and Li (2008); as flux emergence into an active region generally makes for intrusions into one or both polarities of the existing field, flux emergence, flux

cancellation, and displacements involving shearing field are almost unavoidably going on simultaneously (see, e.g., the review by Wang and Liu 2015, with many references to original studies).

These two *MDI-TRACE* studies referenced above already showed that there are regions with distinctly nonpotential coronae without exhibiting SHILs. With the continuous, high-resolution, and full-disk coverage offered by the Atmospheric Imaging Assembly (*AIA*, Lemen *et al.* 2012) and Helioseismic and Magnetic Imager (*HMI*, Scherrer *et al.* 2012) instruments onboard the *Solar Dynamics Observatory* (*SDO*, Pesnell *et al.* 2012), I set out in this study to understand the behavior of the nonpotentiality in active regions in order to evaluate what role the "free energy" linked with this phenomenon can play in flares and eruptions.

Active-region scale nonpotentiality could be caused by electrical current systems attending the flux emergence at SHILs, provided that the distant field corresponding to these currents is not countered by essentially oppositely-directed nearby currents of comparable magnitude. Magnetohydrodynamic (MHD) simulations provide insight into the behavior of twisted flux ropes that emerge from within the convective envelope and currents that are induced by such emergence and by lateral displacements and twisting motions of photospheric field. Manchester *et al.* (2004) and Fang *et al.* (2012), for example, use MHD simulations to show how flux-rope emergence can build up magnetic shear in the corona through shearing flows at the polarity inversion line (PIL) and spot rotation. MHD studies by Török and Kliem (2003), Török *et al.* (2014), and Dalmasse *et al.* (2015) concur in that non-neutralized, i.e. net, electrical currents only occur if the twisting and shearing motions of the flux emergence that they prescribe build up magnetic shear at the PIL. Thus net currents should be expected to form whenever flows extend across the PIL or when the stresses they induce involve flux systems that reach to the PIL.

If the electrical currents linked to, say, M- and X-class flaring and their coronal mass ejections (CMEs) could be inferred to exist based on the apparent nonpotentiality of the most-readily observable loops, i.e., those with lengths roughly comparable to the scale of the active region (including sigmoid configurations, see, e.g., Savcheva *et al.* 2014, and references therein), then a powerful tool would become available for the forecasting of flares and CMEs. Currently, forecasts of flares, and in particular their timing and magnitude, are of poor quality, with skill scores that are hardly positive (e.g. Leka and Barnes 2007; Barnes and Leka 2008). One of the problems that complicate flare forecasting is that the geometry, energetics, and stability of the coronal magnetic field cannot be adequately studied because modeling the field based on surface vector-magnetic data does not, at present, enable reliable extrapolations of the field (see DeRosa *et al.* 2015, and references therein to a decade-long series of team studies of nonlinear force-free field (NLFFF) modeling). The principal issues appear to be not only the intrinsic nonlinearity of the problem, but also the difficulty in inferring all three vector field components in an active region and its surrounding quiet Sun, dealing with an intrinsic 180° ambiguity in the transverse field component that cannot be resolved with single-perspective spectro-polarimetry, the unknown forces acting on the observed photospheric field up to the top of the chromosphere, and the unknown fields at the sides and top of any model volume centered in active regions (problems that similarly hamper the application of the magnetic virial theorem, as discussed by Metcalf *et al.* 2008).

Hoping to mitigate these problems with the use of presently available vector-magnetic data for coronal-field studies, Malanushenko *et al.* (2012) and Chifu *et al.* (2015) developed methods that can combine surface field observations (line of sight and vector fields, respectively) with coronal loop traces to guide the NLFFF modeling (see the application to an active region by Malanushenko *et al.* 2014). As these methods use the set of active-region loops observable in EUV images (such as by *SDO*/*AIA*) we need to understand whether the seat of power for energetic flares and eruptions has signatures in these images that are readily observable and that can be reliably quantified.

In view of these problems, and the above observational and modeling studies, I use *SDO* data in this study to constrain how currents involved in flaring distort active-region coronae away from mostly potential configurations.

2. OBSERVATIONS

For the purpose of this study, I selected solar regions observed by *SDO*/*AIA* from 2010/05 through 2014/10 based on a subjective criterion: all regions within approximately 40° from disk center that appeared substantially nonpotential when comparing a field model with observed loops in the *AIA* 171 Å channel (generally consistent with the 193 Å channel data, not used further in this study). For the latter assessment, I reviewed the daily overlays of PFSS model field lines shown on the *AIA* "Sun In Time" web pages[1]; regions were selected on multiple dates if the criteria of distance to disk center and appearance of nonpotentiality were met. Most regions have NOAA active region numbers, but two (one small, one aged) do not. After this initial selection based on 1645 daily *AIA*-PFSS overlays, I added any regions within 40° from disk center emitting an X-class flare if not already included.

For the selected regions, comparisons of *AIA* 171 Å data and PFSS models were made 1.5 h prior to flares above GOES class M5 in the regions or – if no such flares occurred – 1.5 h prior to the start of a UT date without such flares. The set of 41 selected regions with 78 distinct dates is listed in Table 1.

For each of the entries in Table 1 a 4-day sequence of magnetograms was made, remapped to disk center after removing the differential rotation characteristic of the mean latitude of the target region. Column 4 in Table 1 lists characteristics of the surface magnetic field (in capital letters, sometimes in two or more categories, and between parentheses if weakly or ambiguously), and in the coronal loop configuration in comparison to the PFSS model field (in lower case letters).

For the characterization of the coronal configuration in comparison to the PFSS model field, I use the same qualitative criteria as identified by Schrijver *et al.* (2005). That study characterized the differentiating properties of

[1] `http://sdowww.lmsal.com/suntoday_v2`

Table 1
Selected target regions. Column 2 lists the short-form SOL identifier specifying time of observation (Leibacher et al., 2010), and column 3 the NOAA active region number or, if unnumbered, the (x, y) coordinates relative to disk center in arcseconds. Column 4 lists the dominant behavior for the surface line-of-sight field (capitals) and for the nonpotentiality of the loops in comparison with the PFSS field model (lower case letters), as detailed in Sect. 2; a minus sign following this indicates absence of sunspots or pores, and an asterisk that an eruption preceded the observation with ongoing field evolution. Values of $\log(R)$ (in units of 2.2×10^{16} Mx, see Schrijver [2007] for rationale) are listed as per the algorithm by Schrijver (2007), based on *SDO/HMI* magnetograms scaled to the *SOHO/MDI* resolution as used in that study; for regions with X-class flares, the ratio of R to total absolute flux Φ is also listed. Column 6 lists flares above M5, if any; the GOES flare class is followed by "N" if the flare was non-eruptive as inferred from *SDO/AIA* and SOHO/LASCO observations.

No.	SOL	AR no.	Cat.	$\log(R)$, $\log(R/\Phi)$	Flare(s)	Notes
1	2010-07-01T22:29:00	11084	Eac	2.5	-	Repeated "filament" act. from AR to QS to W, SW
	2010-07-02T22:29:00	"	Eac	0.0	-	Repeated "filament" act. from AR to QS to W, SW
2	2010-08-02T22:29:00	11092	Fab	2.6	-	Erupt's to SW and NE. Cf. Schrijver & Title (2011)
	2010-08-03T22:29:00	"	Fab	0.0	-	Erupt's to SW side
	2010-08-04T22:29:00	"	Fab	2.1	-	Erupt's to SW and NE side
3	2011-02-13T16:00:00	11158	ABc(?)e	4.6	M6.6	-
	2011-02-15T00:26:00	"	Bc(?)e	4.6, -1.4	X2.2	Cf. Schrijver et al. (2011)
4	2011-02-23T22:29:00	$(-64, -95)$	Eab-	0.0	-	-
5	2011-03-09T21:53:00	11166	ABc	4.7	X1.5, -1.5/N	Several large-scale fronts from sides
6	2011-03-27T22:29:00	11176	Abe	3.7	-	Large eruption NW extremity ≈0 UT
	2011-03-28T22:29:00	"	Aabe	3.3	-	Mild activity in interior and towards NE
	2011-03-29T22:29:00	"	Abe	3.3	-	-
7	2011-06-19T22:29:00	11236	Ed	2.4	-	Conf. erupt's ∼2:30, ∼12:30, ∼16:30, ∼18:30 UT
	2011-06-20T22:29:00	"	Ed	2.9	-	Conf. erupt's ∼7:00, ∼18:30, ∼22:00, ∼23:30 UT
8	2011-06-23T22:29:00	W of 11240	Cac-	0.0	-	No notable impulsive events on 2011/06/23
9	2011-09-06T20:50:00	11283	Bc	4.1, -2.0	X2.1	-
	2011-09-07T21:08:00	"	Bcd	4.0, -2.0	X1.8	Associated with eruption of cool material
10	2011-09-13T22:20:00	11289/-93	E(C)cde*	3.8	-	Large eruption and post-erupt. loops at end of day
11	2011-10-27T22:29:00	11330	Cae	4.0	-	Large QS eruption on the N to NW side ≈midday
	2011-10-28T22:29:00	"	Cade	4.1	-	Eruption on NE side ≈16 UT
12	2011-12-02T22:29:00	11362	ACe	3.5	-	No notable impulsive events on 2011/12/02
	2011-12-03T22:29:00	"	ACe	3.5	-	Internal act. ≈05 UT and in N-periphery ≈14 UT
	2011-12-04T22:29:00	"	Ce	2.8	-	Internal act. ≈16 UT
13	2012-01-18T22:29:00	11399	Ebc*	0.0	-	During afterglow of a long AR-QS filament eruption
14	2012-03-06T22:54:00	11429/-30	BCbce	5.0, -1.2	X5.4/X1.3	Frequent activity within -29 and in loops to -30
	2012-03-08T22:29:00	"	BCbce	4.7	-	Quiescent (but with data gaps)
	2012-03-09T22:29:00	"	Bbce	4.6	-	Major eruption ≈ 3 UT
15	2012-03-28T22:29:00	11442	Cbce	3.4	-	Recently emerged next to existing bipolar region
16	2012-05-03T22:29:00	11470/-1/-2	(C)abe	3.3	-	Moderate mostly confined eruption ≈11:30 UT
	2012-05-04T22:29:00	"	Eabe	0.0	-	Possible eruption ≈15:30 UT
	2012-05-05T22:29:00	"	Ebe	3.3	-	Large eruption ≈ 06 UT
17	2012-05-28T22:29:00	11490	Ce	3.9	-	Fast QS coronal evolution on leading side ≈ 11 UT
	2012-05-29T22:29:00	"	C(a)e	3.5	-	Fast QS coronal evolution in leading region ≈11 UT
18	2012-06-04T22:29:00	11497	Dae	2.1	-	[Missing *AIA* daily movies]
19	2012-07-10T04:01:00	11519/-20/-1	BCbc	4.8	M5.7	Also frequent moderate activity
	2012-07-11T22:29:00	"	Bbe	4.3	-	Frequent moderate activity
	2012-07-12T15:19:00	"	Bbe	4.8, -2.1	X1.4	Also frequent moderate activity
20	2012-07-31T22:29:00	11532/-36	Cabe	3.9	-	-
	2012-08-01T22:29:00	"	Dabe	3.6	-	-
	2012-08-02T22:29:00	"	Gabe	3.4	-	-

evolving surface magnetic field for the sets of nonpotential and mostly potential regions. Quoting directly from that study (including percentages that were given for the fraction of regions with such characteristics, sometimes in multiple categories):

A (71% of all nonpotential cases): field is still emerging, or was within the last day, with meandering or fragmented polarity separation lines, associated with sustained shearing motions of the field as it sorts itself out; in some cases this leads to nonpotential fields low down while leaving the largest scales nearly potential;

B (43%): there are touching and rapidly evolving (canceling) opposite polarity concentrations of high flux density up to ∼ 30 h earlier, unless that is a small part of the overall flux in the region; if these form a relatively small and compact fraction of the overall active region, the nonpotentiality is weak or limited to that compact region;

C (14%): field emerges within or adjacent to an existing configuration, provided it introduces significant new flux, and does not have a neutral line shared with that of the pre-existing field.

They also note that the (near-)potentiality of the overlying field is not (necessarily) affected if (quoting again):

D (41% of all near-potential cases): strong mixed-

Table 1
(cnt'd)

No.	SOL	AR no.	Cat.	log(R), log(R/Φ)	Flare	Notes
21	2012-08-11T22:29:00	11542	Fa*	3.9	-	Eruption ≈16:30 UT
22	2012-09-01T22:29:00	11555/-60/-61	Cbce*	4.3	-	Frequent eruption from region and nearby
23	2012-09-17T22:29:00	11569/-71/-74	E(C?)ae	2.9	-	-
24	2012-10-28T22:29:00	11599	-a	0.0	-	Isolated spot, no sign. coronal activity
25	2012-11-29T22:29:00	11621	EGde	2.3	-	Only limited activity
	2012-11-30T22:29:00	"	EGde	2.3	-	Only limited activity
	2012-12-01T22:29:00	"	EGde	1.8	-	Only limited activity
26	2012-12-02T22:29:00	11623/-25	Cabe	2.0	-	No substantial activity
	2012-12-03T22:29:00	"	Ebe	3.2	-	No substantial activity
27	2012-12-19T22:29:00	11633/-4	Ga	3.6	-	Moderate erupt's AR 11633 ≈02, 10, 18, & 24 UT
28	2013-05-17T22:29:00	11745	Fce	2.6	-	-
	2013-05-18T22:29:00	"	Fce	2.3	-	-
29	2013-06-10T22:29:00	(163, 38)	Eabe-	1.5	-	-
	2013-06-11T22:29:00	"	Eabe-	0.0	-	-
30	2013-10-13T22:29:00	11864/-5	Abc*	4.2	-	Eruption ≈00:30 UT and ≈20 UT
	2013-10-14T22:29:00	"	Cbc	4.1	-	Erupt. ≈13 UT, and from leading flux ≈16:30 UT
31	2013-11-08T02:56:00	11890	Cc	4.5, -1.9	X1.1	Compact intrusion at trailing polarity
	2013-11-10T03:44:00	"	Cd	4.3, -1.9	X1.1	Compact intrusion at trailing polarity
32	2013-11-14T22:29:00	11895/-7	Ccde	4.3	-	-
	2013-11-15T22:29:00	"	Ccde	4.1	-	-
	2013-11-16T22:29:00	"	Ccde	4.0	-	Eruption ≈08 UT
	2013-11-17T22:29:00	"	Ccde	3.8	-	Repeated jet-like activity
	2013-11-18T22:29:00	"	Ede	3.0	-	Some moderate activity
33	2014-01-07T17:02:00	11944	Cae	4.7, -1.8	X1.2	X-flare not over high-gradient field. Conn. to 11946
34	2014-01-08T22:29:00	11946	Aae	3.4	-	Moder. internal act. and northward. Conn. to 11944
35	2014-01-13T22:29:00	11950	Ea	2.8	-	QS filament eruption trailing AR
36	2014-02-06T22:29:00	11970	G(C?)bce*	2.7	-	Signs of eruption ≈21 UT
37	2014-03-29T17:48:00	12017	ABc	4.3, -1.7	X1.0	Preceded by at least two flares/eruptions
38	2014-05-25T22:29:00	12071/-3	Cb	2.9	-	-
	2014-05-26T22:29:00	"	Cc	2.9	-	-
39	2014-06-16T22:29:00	12090	Ea	2.7	-	-
	2014-06-17T22:29:00	"	Ea	2.2	-	-
40	2014-09-10T16:15:00	12158	Gcd	4.3, -1.8	X1.6	Moderate activity in and around AR
41	2014-10-22T12:58:00	12192	Ad	5.1, -1.5	X1.6/N	Very active; see text
	2014-10-23T08:20:00	"	Ad	5.0	M1.1/N	Very active; see text
	2014-10-24T20:16:00	"	Ad	5.1, -1.7	X3.1/N	Very active; see text
	2014-10-25T15:38:00	"	Cd	5.1, -1.6	X1.1/N	Very active; see text
	2014-10-26T09:26:00	"	Bd	5.2, -1.5	X2.0/N	Very active; see text

polarity emergence has strongly decreased in the last $10-20$ h, or when such emergence is just starting;

E (36%): the configuration is that of a simple, gradually-evolving bipole;

F (18%): flux cancels rapidly in a mature or decaying region having a simple bipolar configuration with a relatively straight and well-defined polarity inversion line;

G (5%): relatively small bipoles emerge within an existing active region, regardless of their position relative to the neutral line.

For the present study, the deviation of *AIA* coronal loops from the PFSS model is characterized in five classes that are complementary only to a limited degree:

a) in a large-scale swirl in loops from one or more major flux concentrations;
b) in large-scale loops system essentially connecting the two main polarity regions:
c) in low-lying coronal emission structures or chromospheric absorption structures;
d) in a small set of loops at a relatively small segment of the AR corona;
e) in loops connecting to surrounding active regions or distant quiet Sun.

Table 1 also lists the total flux in the vicinity of the strong-field, high-gradient polarity inversion lines (denoted below as SHILs) associated with the active region (or active region complex if in close proximity) as introduced by Schrijver (2007) (giving the value of log(R) in the fifth column of the table), and the largest flare on a given date provided of GOES class M5 or larger[2].

Many of the selected regions, in particular those exhibiting X-class flares, have been analyzed in the literature. The subsections below review that work[3] where

[2] Supporting electronic materials are available at `http://www.lmsal.com/nonpotential/`, including links to the *SDO* SunToday pages, remapped magnetogram sequences, log($R(t)$ diagrams, the PFSS field line overlays on magnetograms and *AIA* 171 Å images, and *AIA* daily summaries.

[3] Literature studies were identified using iSolSearch [`http://lmsal.com/isolsearch`] which can perform ADS queries

pertinent to this study, adding some comments to complement or clarify entries in Table 1 and Figs. 1-6.

2.1. *AR 11084*

The nonpotentiality of the corona over AR 11084 (shown in the bottom panels of Fig. 1) was also shown by Komm *et al.* (2014), who noted that it persisted for the entire disk passage. This region has well-separated polarities, exhibiting nonpotential signatures most clearly in the counterclockwise spiral in the loops emanating from the leading spot. Although the region does not exhibit M- or X-class flaring (not expected for a region of this flux content), it does show repeated activity within it in connections to the quiet Sun on the west and southwest.

Liu *et al.* (2013) found that the flows around AR 11084 at the surface and at a rather shallow depth of 500 km were quite similar, although somewhat different in horizontal extent. Komm *et al.* (2014) used ring-diagram analysis to find a predominant kinetic helicity in the subsurface flows, but the connection with the coronal nonpotentiality remains unclear, because two of their six control regions without "persistent whirl patterns" in chromospheric and coronal images also showed kinetic helicity of one predominant sign.

2.2. *AR 11092*

Activity in and around AR 11092 was described for 2010/08/01 and 02 by Schrijver and Title (2011), who focused on the long-range couplings between the fields involved, including likely influences from emerging flux on the far hemisphere on the flaring of the region and the destabilization of neighboring quiet-Sun filaments.

Liu *et al.* (2013) map the flows around AR 11092 in photospheric and subphotospheric layers to find similar flows at different depths around the main sunspots. The flow patterns around the area of flux emergence, in contrast, are quite different: the characteristic surface features of separation of polarities, rotation of the sunspots, and shear along the polarity-inversion line do not appear to have counterparts at depth.

As for AR 11084, Komm *et al.* (2014) noted a persistent nonpotential swirl in the field over the leading spot of AR 11092, and also here find a predominant kinetic helicity in the subsurface flows.

2.3. *AR 11158*

The region (Fig. 2, top), has signatures of nonpotentiality mostly in its interior and in a few long loops connecting outward from the interior of the region. Overall, the compatibility of *AIA* 171 Å loops and PFSS field lines is quite difficult to assess. Loop bundles on the southern side, for example, are not outlined by field lines, but this could be a sampling problem. Clearly, there is no dominant swirl in loops from either of the dominant flux clusters at the region's ends.

AR 11158 produced the first X-class flare (X2.2) of the current sunspot cycle, a flare that was the first of its class observed by *SDO/AIA*. This event consequently received much attention in the literature, starting with Schrijver *et al.* (2011). Toriumi *et al.* (2014) (see also Janvier *et al.* 2014) describe the evolution of the surface field of the region and of its coronal configuration up to the point of the X2.2 flare. They apply MHD modeling of the flux emergence to gain insight into the formation of the highly-sheared strong-field polarity inversion line involved in the onset of the flare and coronal mass eruption. Based on these simulations, they argue that the region, with a surface appearance of two adjacent emerging bipolar regions, was formed from a single subsurface structure that fragmented during its rise (see also Chintzoglou and Zhang 2013). The interaction between two opposite-polarity flux bundles in a glancing collision created the strongly-sheared high-R PIL conditions (see also Wang *et al.* 2013) that they suggest enabled the formation of a flux rope that appeared to play a key role in the observed flare and CME (see also Inoue *et al.* 2015).

The existence of such a flux rope is consistent with work by Malanushenko *et al.* (2014) who use the coronal loops observed by *AIA* in combination with the surface magnetic field to compute a NLFF field. They note: "Immediately prior to the eruption, the model field contains a compact sigmoid bundle of twisted flux that is not present in the post-eruption models". The study by Petrie (2013) shows that the high-R PIL, and in particular structures around the end points of the inferred flux rope, are locations where the horizontal field component increased (also noted by Sun *et al.* 2012), and the Lorentz force shows the most pronounced change when comparing pre- and post-flare vector magnetograms (also seen in flares in ARs 11166, 11283, and 11429 described in subsequent sections, see Petrie 2012)

The sunspot linked to the X2.2 flare was rotating, as was another adjacent to an M2.2 flare on the day before: Li and Liu (2015) note that the M2.2 flare occurs when the spot rotation rate peaks.

Kazachenko *et al.* (2015) estimate Poynting fluxes in a 6-day sequence of photospheric vector-magnetic maps observed by *SDO/HMI* to conclude that the estimated free energy of $\approx 2 \times 10^{32}$ erg is compatible within better than a factor of two with the energy needed for the X-class flare on 2011/02/15 and with other estimates of the free energy (see references in their paper).

2.4. *Region no. 4*

This unnumbered spotless region (located at $(x, y) = (-60, -96)$ arcsec from disk center at the selected time) is shown in the top panels of Fig. 3. It has a counterclockwise spiral from its leading polarity flux deviating strongly from the PFSS model field. There are no signs of flux emergence in the four days leading up to the time selected for this study (picking up the region at 60 degrees East). The *SDO/AIA* summary movies[2] show no substantial eruptive activity on the date selected.

2.5. *AR 11166*

The active region-scale loops in the *AIA* 171 Å image are not unambiguously nonpotential, so this region was not selected based on its nonpotentiality, but was added for review because of the X-class flare within it. Some loops within the deep active-region interior do appear to reflect nonpotentiality.

Vemareddy *et al.* (2012) describe the magnetic evolution of AR 11166 (and of 11158) in the days leading up to the X-class flare, describing the shearing caused by

for papers with AR numbers in title or abstract.

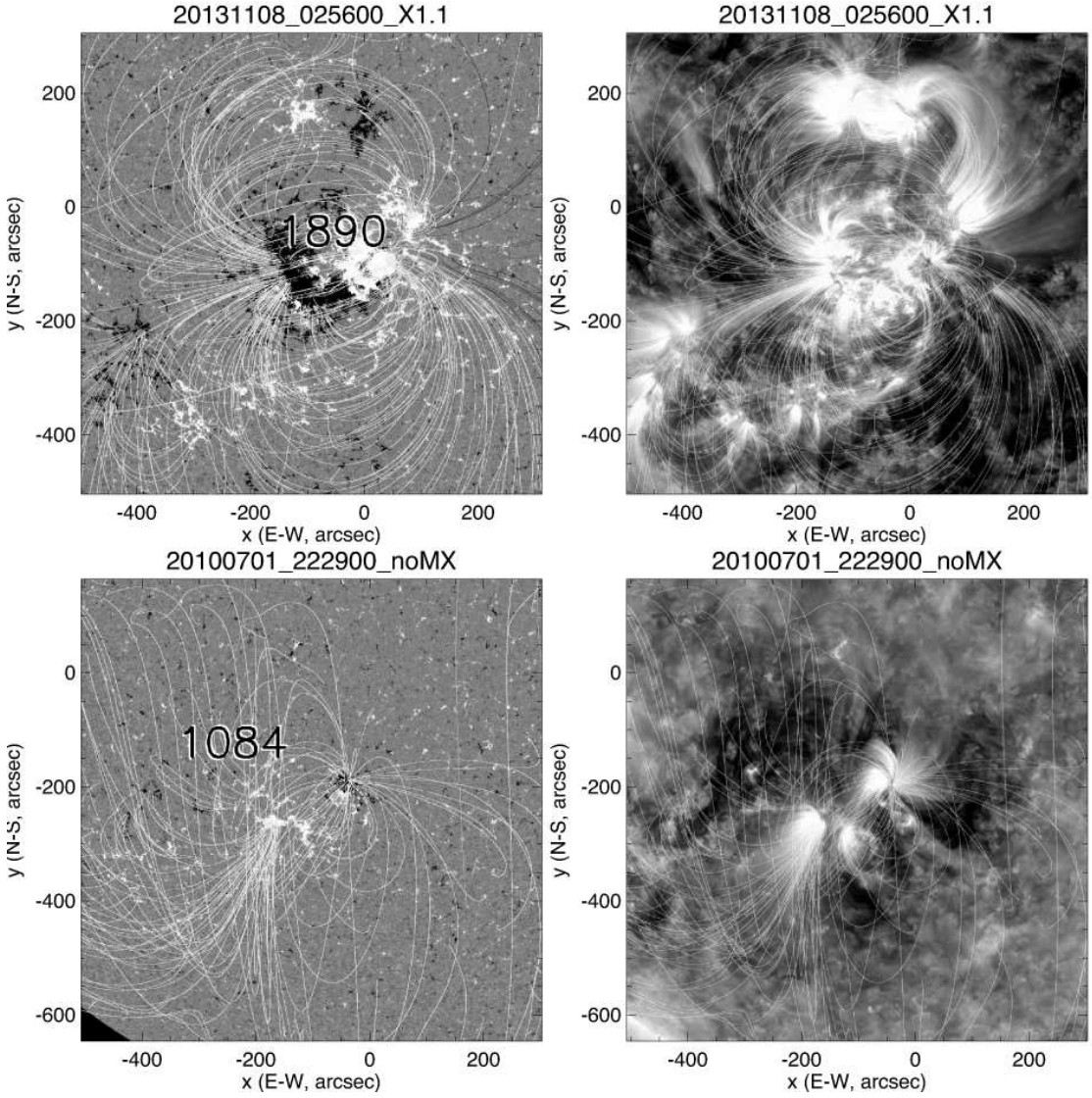

Figure 1. Example regions in category 'c', with and without X flares: *(top)* AR 11890 *(bottom)* AR 11084. Each panel shows a field of view of 810 arcsec (1350 image pixels) to a side. Left panels: *HMI* magnetograms (with the positive and negative polarities - shown in white and black, respectively - saturating at $\pm 75\,\mathrm{Mx/cm^2}$) with PFSS field lines overlaid (white if closed, dark if "open" to the heliosphere, i.e. if connecting to the source surface); the probability of starting field lines at a give location increases with increasing flux density. Only the last four digits of the AR number are shown, following the standard practice at NOAA's Space Weather Prediction Center. Right panels: *AIA* 171 Å images with the same field lines blended in.

the relative motions of the opposite polarity flux concentrations. See Vemareddy and Wiegelmann (2014) for a description of the X1.5 flare and NLFFF field modeling.

The magnetogram sequence suggests that the high-R PIL in the interior of the region formed largely as a result of the displacement of emerging flux in the SE periphery of existing flux, with the leading polarity moving towards the west and eventually northward, compressing and shearing opposite polarities.

2.6. *AR 11283*

There is apparent nonpotentiality in the interior and likely on the northwest perimeter of the region, but not obviously so in the active-region scale loops.

Flaring is connected to compact flux emergence north of the leading sunspot. The X1.8 flare on 2011/09/07 is notable because of a substantial amount of chromospheric material being ejected. The field evolution around the time of the two X-class flares was described by Ruan *et al.* (2014, 2015). These studies note that both major flares were associated with clear sunspot rotation. The SHIL involved in the flaring started to form with flux emergence from about 2011/09/03 09 UT onward, i.e. for some 3.5 days prior to the first X-class flare. The flux emergence, on the north-west side of the leading sunspot, pushed the trailing, positive (rotating) polarity into pre-existing spots, while remaining connected to the leading polarity moving ahead of the region while connected by a filament and – in the NLFFF model – a flux-rope structure. Ruan *et al.* (2015) note that whereas the polarities of the intruding bipole continue to separate, "no apparent flux emergence is observed during the period between the X2.1 and X1.8 flares," and that a filament configuration persisted after the X2.1 event.

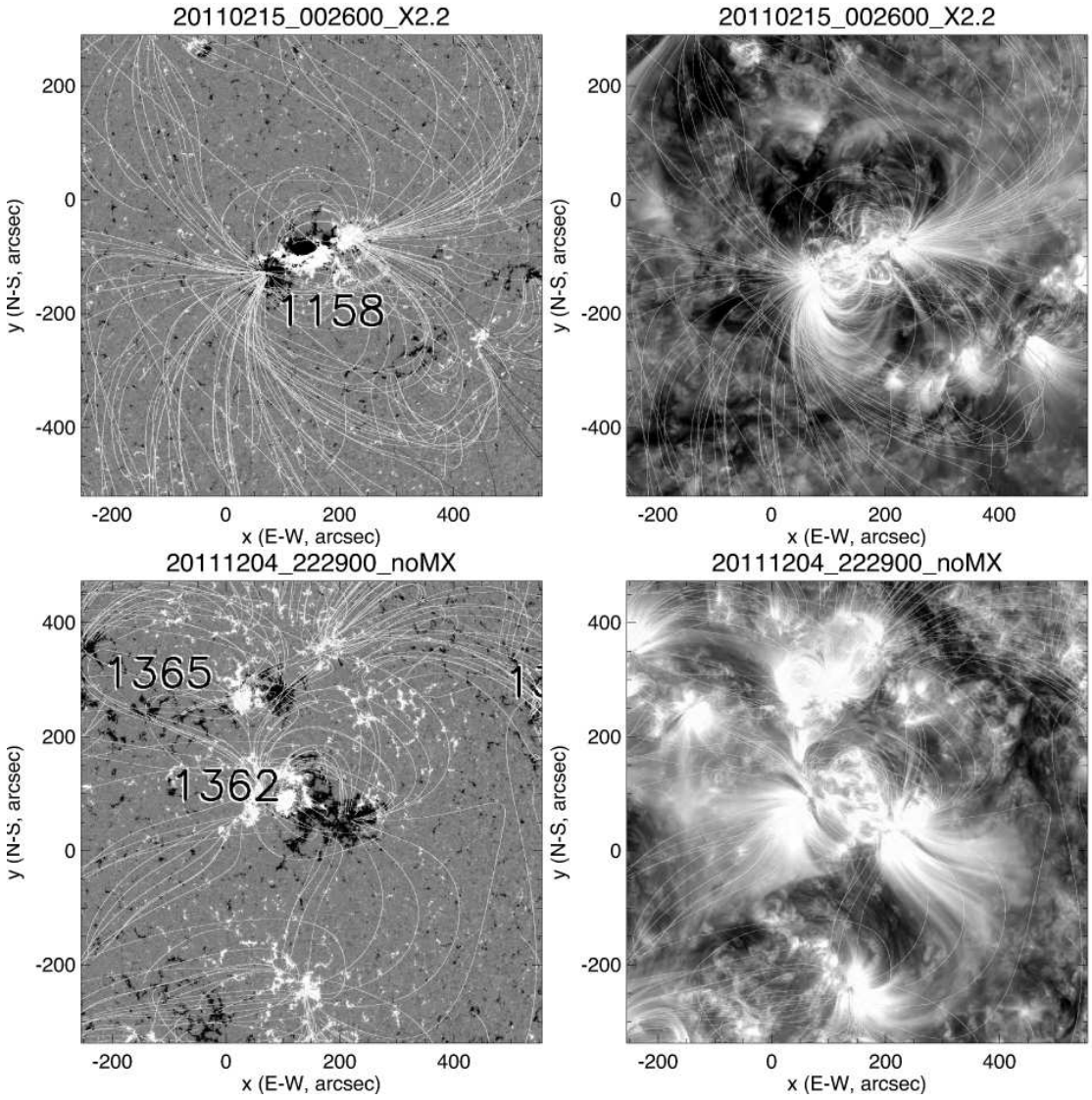

Figure 2. As Fig. 1: Example regions in category 'e', with and without X flares: *(top)* AR 11158 *(bottom)* AR 11362.

2.7. *AR 11289/-93*

The *SDO*/*AIA* observations suggest a large eruption from these regions in the final hours of 2011/09/13, but with no major flaring, although there are apparent post-eruption loops for the first ≈ 6 hrs of 2011/09/14. The loops arching equatorward are most inconsistent with the PFSS field model.

2.8. *AR 11362*

The region, shown in the bottom panels of Fig. 2, has apparent nonpotentiality in loops from its leading polarity that connect to a decayed region to the south.

A mid-sized bipolar region emerges to the north, starting around 2011/12/01 21 UT, ending its flux increase at the end of 2011/12/03. This causes coronal deformation in the northern reaches of AR 11362 around 2011/12/03 14 UT, and more on the 4th, with also what is likely an eruption from AR 11362 around 16 UT on that day.

2.9. *AR 11429/-30*

The region (Fig. 4 top) exhibits nonpotentiality in connections to a decayed region to the south as well as towards the north, and likely in loops emanating from its interior. Note also the counterclockwise swirl from the trailing polarity of the region just ahead of it, AR 11430.

Leading AR 11429 is a newly emerging flux region, starting around 2012/03/04 05 UT, which becomes AR 11430. AR 11429 exhibits frequent activity, both within the region, and in the evolving connections to AR 11430 on 2012/03/06. There appears to be much less activity on 2012/03/08 (but note that *AIA* coverage on 2012/03/08 misses multiple hours), but there is a major eruption on 2012/03/08 after 03 UT.

Internally, AR 11429 has a long SHIL, being maintained for the selected date range by sustained shearing and converging displacement of the fluxes around it.

Chintzoglou *et al.* (2015) describe the evolution of AR 11429 from 2012/03/05 to 2012/03/08, including the evolution of a rope structure above the SHIL, the sunspot rotation, coronal activity, and two fast CMEs (exceeding 2000 km/s) in essentially opposite directions that oc-

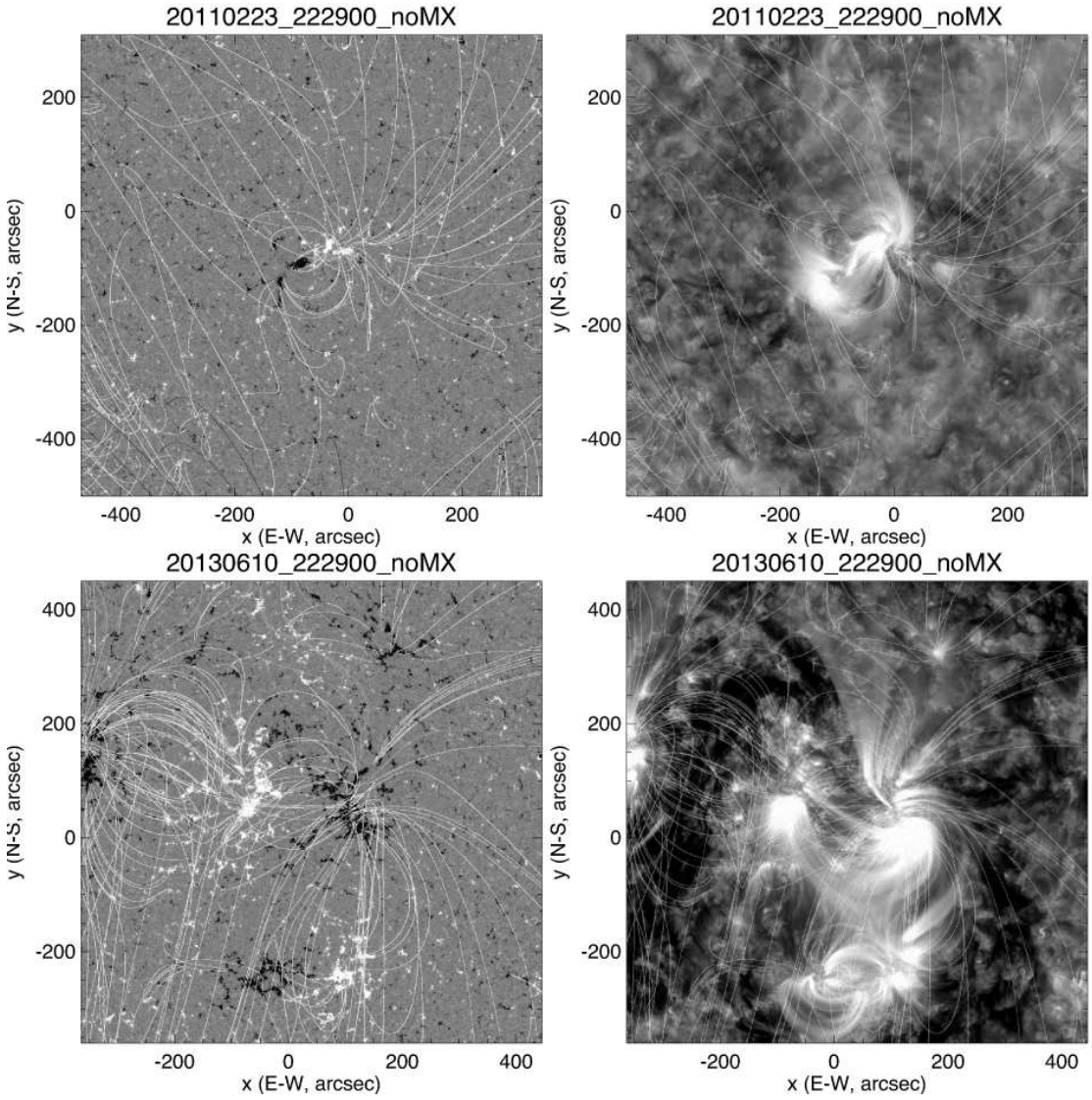

Figure 3. As Fig. 1: Unnumbered spotless regions, both without major flaring: *(top)* region no. 4 *(bottom)* region no. 29.

curred early on 2012/03/07 in association with the X5.4 and X1.3 flares. Their NLFFF extrapolation for late on the 2012/03/06 contains a weakly-twisted flux rope configuration along the length of the primary PIL that they argue is composed of two segments, each one of which involved in a separate flare and related CME.

2.10. *AR 11519/-20/-1*

This area is a complex of three substantial, closely-packed active regions, with flux emergence throughout, which hampers the assessment of is nonpotentiality. Loops on the northern, trailing side of AR 11520 are inconsistent with the PFSS field lines, as are low-lying chromospheric (absorption) features in the 171 Å image. The leading AR 11521 does not start to emerge until $\approx$ 15 UT on 2012/07/08 continuing until about 2012/07/09 18 UT. The main SHIL in AR11519 is sustained by converging motions of the main flux clusters.

2.11. *AR 11555/-60/-61*

This is a group of bipolar regions in which AR 11561 begins to emerge on 2012/08/29 around 06 UT until the moment selected for this study, with polarity mixing in its interior. There is a cluster with multiple internal loop sets that is suggestive of nonpotentiality.

A very large and extended quiet-Sun filament eruption occurs towards the southeast of the region, of which the leading end connects to loops from AR 11561. That region exhibits a possibly induced eruption on its leading edge around 20:30 UT on that day, followed by another at 22 UT, then again on 2012/09/01 around 01 UT, 05:30 UT, 09 UT, and 12:30 UT, with another from the region to the north around 18 UT.

2.12. *AR 11623/-25*

ARs 11625 and 11623 are a pair of comparable sizes, perfectly aligned next to each other, 11625 to the north of 11623. On 2012/11/29, AR 11625 is still emerging, but by the end of that day, polarities are separating. The region, shown in the bottom panels of Fig. 4, is most clearly inconsistent with the PFSS field model in

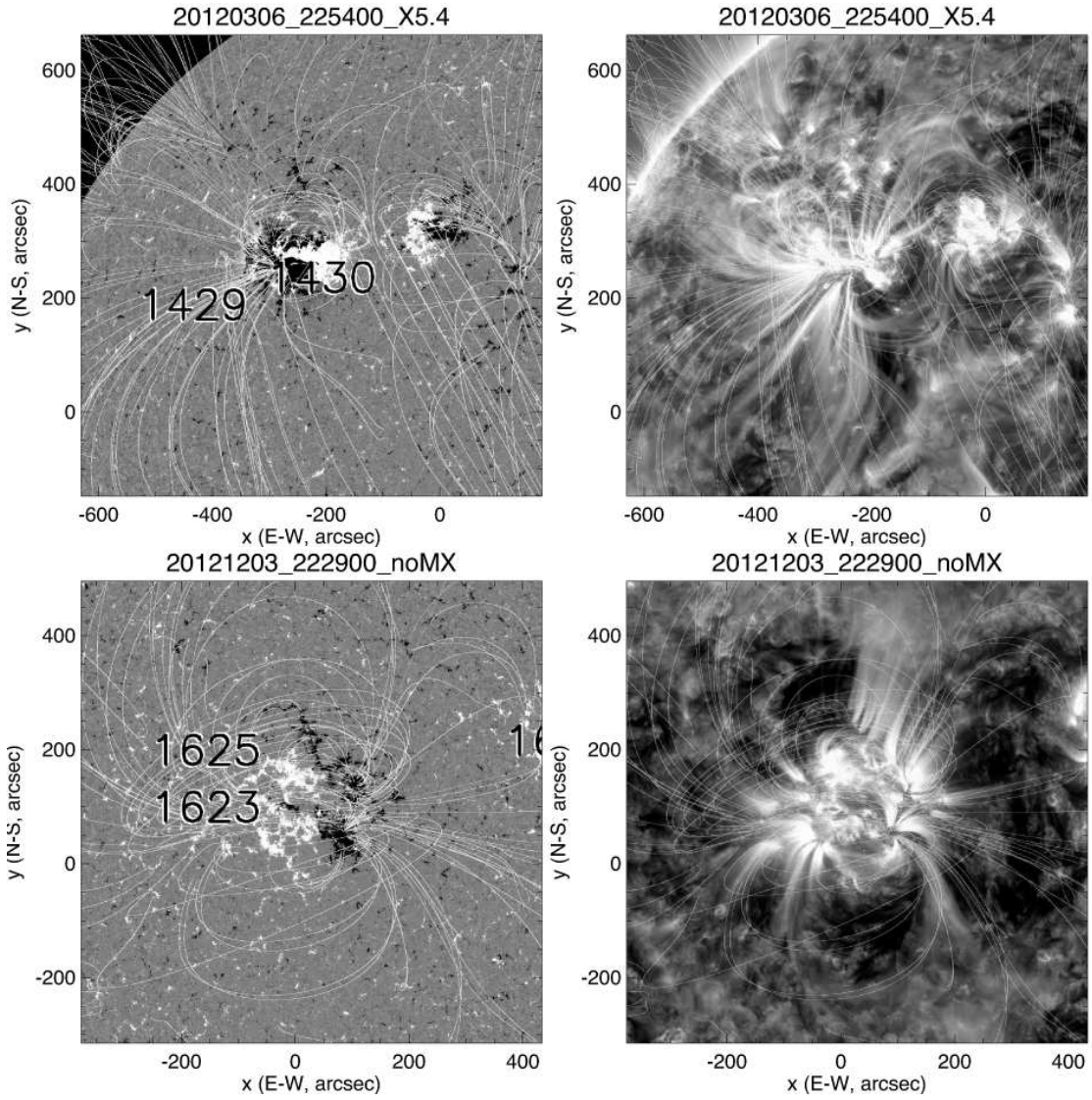

Figure 4. As Fig. 1: Example regions in category 'b': *(top)* AR 11429/-30 *(bottom)* AR 11623/-25.

loops emanating from the leading polarity of the northern region (AR 11625).

2.13. *Region no. 29*

This region, located at $(x, y) = (42, 45)$ arcsec from disk center on 2013/06/10 (shown in the bottom panels of Fig. 3), has a strong clockwise swirl in the loops from its leading polarity that differ markedly from the PFSS model field. It is a decaying bipole, with both polarities broken up in supergranular flows, and well separated.

2.14. *AR 11864/-5*

This region has possibly nonpotential loops in its interior. There is an eruption from the trailing part of the flux complex around 00:30 UT, and a coronal evolution that could be another eruption around 20 UT with loops continuing to reshape until beyond the end of the day on 2013/10/13, then another eruption on 2013/10/14 around 13 UT, and one from the leading flux cluster at ≈16:30 UT with loop deformations continuing until past the end of the 14th.

2.15. *AR 11890*

The region (Fig. 1, top) has no obvious signs of nonpotentiality in its overall appearance, although the leading spot shows signs of a counterclockwise swirl.

The X flares occur over compact flux emergence with strong shear flows at the trailing end of the region, with both flares displaying pair of nested post-eruption loop arcades as expected for the multipolar area involved in the flares. Loops around that area do not obviously disagree with the PFSS model.

2.16. *AR 11895/-7*

There are possible signs of nonpotentiality in loops from the leading polarity of AR 11895.

Shearing of a high-R region appears to exist when AR 11895 is near the limb, but this fades early on the 12th; by the 14th the region has largely separated polarities, with a large leading spot well ahead of the remainder of the leading polarity flux that is already largely fragmented, as is the trailing polarity.

The region shows no substantial activity until an erup-

tion on its northern side on 2013/11/16 around 08 UT with subsequent loop evolution lasting until the end of the day. On the 17th, continuing subdued on the 18th, there is frequent small-scale activity with jet-like eruptions from the southern side of the trailing polarity, likely associated with flux emergence into the area.

2.17. *AR 11944 and AR 11946*

The flaring region, AR 11944 (Fig. 5, top) is not obviously nonpotential, although the loops from the leading spot shows a very pronounced counterclockwise swirl. Loops in the core region of AR 11944 also exhibit nonpotentiality. Moreover, the neighboring small AR 11946 is nonpotential, judging from the counterclockwise spiral of its trailing polarity.

There are multiple high-gradient regions contributing to the region's R value, reflecting compact flux emergence, convergence, and cancellation in the region's interior along the overall PIL. Northward of the region, a new bipolar region begins to emerge round 2014/01/03 22 UT, continuing throughout the next few days; emergence ends around 2014/01/08 when the polarities are separated around 03 UT. This emerging region, AR 11946, is well connected to AR 11944, in particular visibly to the leading sunspot from which loops exhibit a counterclockwise swirl. The X flare originates from under a loop system to the south of that. This is an unusual eruption of field connecting a large leading spot with dispersed trailing field of old AR on the leading side. *AIA* 304 Å observations suggest filament involvement. Note that no high-R region appears to be connected to the X flare.

2.18. *AR 12071/-3*

AR 12071 is largely complete showing little flux emergence, but AR 12073 has strong flux emergence for several days intruding into an existing bipole. The leading spot of the latter persists, and spot and flux of the new emergence move towards it and appear to be deflected southward just prior to merging with it. There is a nonpotential swirl over the leading polarity of AR 12071.

2.19. *AR 12158*

This is a strong, compact region with most likely moderate nonpotential loops particularly from the southern/trailing polarity (suggesting a clockwise swirl), as well as for loops from the leading edge of the southern/trailing polarity. The X-class flare involves a long, curved filament riding on the PIL, clearly indicating sheared field, involving a few relatively small SHILs in three patches along its length. There is considerable activity and emergence in its moat region, particularly towards the south, pushing into the trailing polarity.

2.20. *AR 12192*

AR 12192 is a very well studied region, attracting considerable attention because it exhibited a series of 6 X-class flares none of which had a corresponding CME. There were another 29 M-class flares of which only one, originating from the periphery of the region (where 5 other M flares occurred), was associated with a CME (Chen *et al.* 2015). See Sun *et al.* (2015) for further discussion and interpretation of why this region exhibits so many energetic confined flares.

At the time studied here, the region is mostly formed, but there is much ongoing flux emergence, including shearing motions and densely packed opposite polarities in at least four places scattered around the main PIL.

The region, shown in the top panels of Fig. 6, is clearly nonpotential in some loops from its trailing polarity, and has multiple chromospheric (absorbing) fibrils and filaments suggestive of sheared field. But the appearance of the other active region-scale loops is not unambiguously nonpotential, and even nonpotentiality in the core appears limited (Sun *et al.* 2015).

3. DATA ANALYSIS AND REVIEW

The observations summarized above show that high-energy X-class flares and pronounced nonpotentiality as inferred from loops observed in the *AIA* 171 Å or 193 Å channels are only moderately correlated: only six of ten active regions with X-class flares exhibit clear signs of nonpotentiality in region-scale loops, while clearly nonpotential regions do not necessarily display significant flaring (or major eruptive activity).

Examples of nonpotential regions without major flaring include AR 11176 (with $\log(R) = 3.3$), AR 11362 ($\log(R) = 3.5$), ARs 11569/-71/-74 ($\log(R) = 2.9$), AR 11621 ($\log(R) = 1.8 - 2.3$), AR 11745 ($\log(R) = 2.3 - 2.6$), AR 12071/-3 ($\log(R) = 2.9$), and AR 12090 ($\log(R) = 2.2 - 2.9$), as are the two spotless (and consequently unnumbered) regions.

In some cases, nonpotentiality may be a temporary signature of a preceding eruption from which the coronal field is still relaxing (regions marked with an asterisk in Table 1). The post-eruption reconfiguration of the higher coronal configurations can take many hours (see, e.g., Schrijver *et al.* 2013). In one such case, AR 11399, the loop system is reflecting the afterglow of a large filament reconfiguration extending from the AR into distant quiet Sun that started at the end of 2012/01/17 (with an eruption that was not observed, occurring during one of the infrequent *SDO* off-point maneuvers), and continuing loop evolution and afterglow until past the end of the selected date. Similarly, AR 11542 erupted around 16:30 UT on the selected date, with sustained afterglow of the loops at least until around 22 UT, so this region, too, may still be relaxing from an eruption. Also AR 11289/-93 exhibited a large eruption in the final hours prior to the selected time, with afterglow continuing for at least some 6 h into the next day. ARs 11555/-60/-61 also are observed between eruptions, with one preceding the selected time by only about half an hour. And ARs 11864/-5 appears to be still reconfiguring after an eruption. Possibly even AR 11970 is subject to the same: a slow coronal change, reminiscent of an eruption, occurred around 21 UT with some continuining evolution for a few hours afterwards.

In cases like AR 11519/-20/-21 the corona may be very complex and dynamic and a moderate-resolution PFSS field model could be inadequate to approximate the appropriate potential-field model.

For other cases, in which the photospheric field is simply structured and the corona not particularly dynamic, there is no obvious pattern in an instantaneous magnetogram to infer the degree of nonpotentiality. Regions without large flares on a given day can appear strongly nonpotential even when the polar-

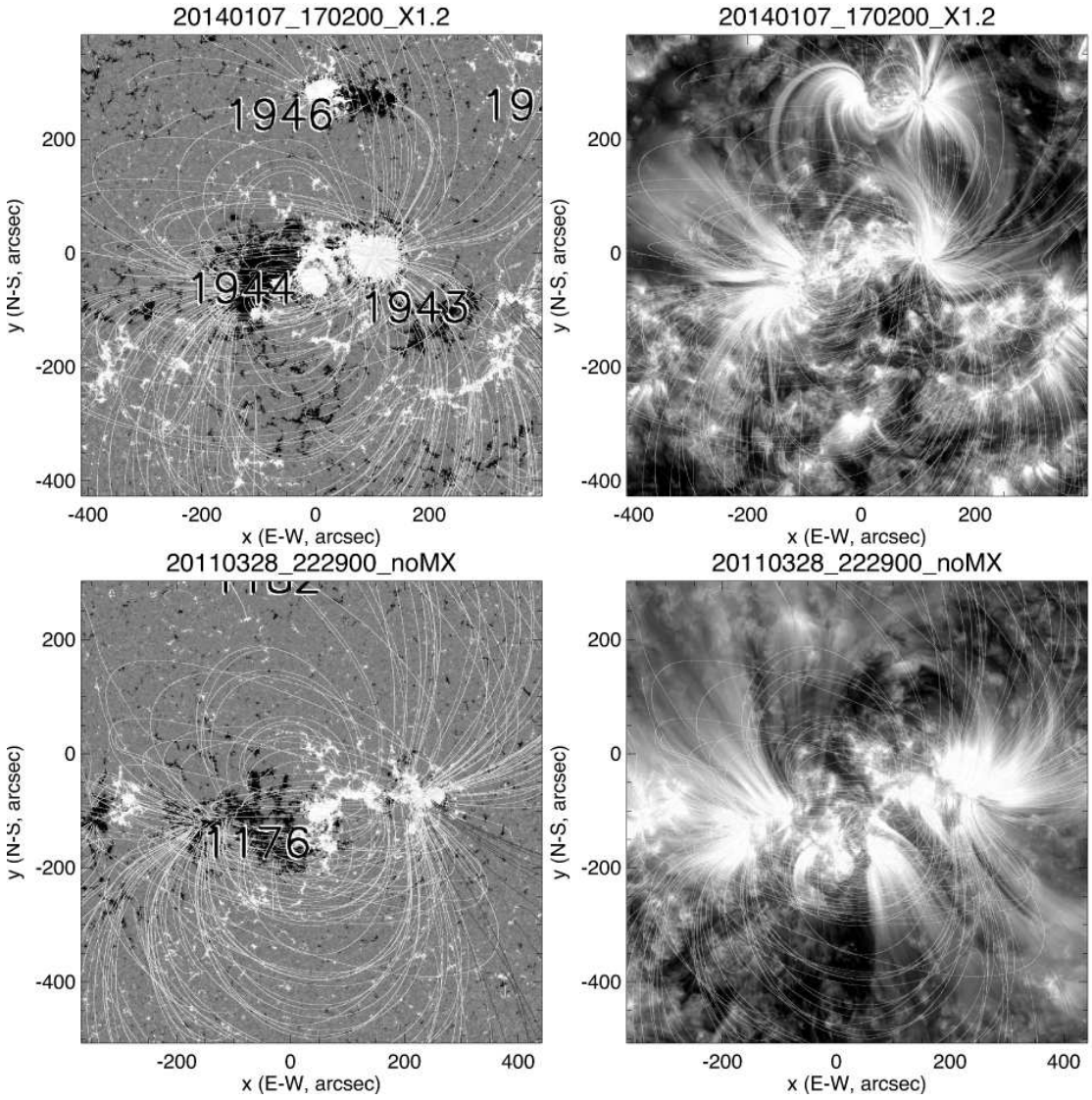

Figure 5. As Fig. 1: Example regions in category 'a', with and without X flares: *(top)* AR 11944 *(bottom)* AR 11176.

Table 2
Contingency table for $\log(R)$ measuring the unsigned SHIL flux associated with flaring in excess of M5 in the sample.

No. of regions:	no M or X	M or X
$\log(R) \leq 4.0$:	49	0
$\log(R) > 4.0$:	11	18

ities are moderately to well separated; see, for example, AR 11092 ($\log(R) = 2.6$), AR 11236 ($\log(R) = 2.4 - 2.9$), AR 11362 on 2011/12/02-04 ($\log(R) = 2.8 - 3.5$), AR 11399 ($\log(R) = 0$), AR 11497 ($\log(R) = 2.1$), and AR 11542 ($\log(R) = 3.9$), or they may have a predominantly bipolar configuration with some satellite regions (such as AR 11330, AR 11240 and preceding region, and the unnumbered region on 2011/06/23). Nonpotentiality for such regions may even be evident in case one polarity has largely dispersed and cancelled, leaving a predominantly single polarity region. The clearest example of this is AR 11599, but AR 11621 and AR 12090 are to some extent comparable: their trailing polarity still exists, but is distant from the large leading spots that contain essentially all of the leading-polarity flux. Other nonpotential regions have a multipolar structure (such as AR 11176, and AR 11895/-97). Some (e.g., AR 11442, ARs 11470,-71,-72, ARs 11555/-60/-61, ARs 11569/-71/-74, ARs 11614/-16/-19) show nonpotentiality in the connections between fairly-well separated satellite regions, or even regions so dispersed they are essentially enhanced network (AR 11490).

Dynamics of the field may be more telling: regions with magnetic field patterns that have little recent flux emergence, well separated polarities, simple bipolar configurations (i.e., categorized in classes D-G defined in Sect. 2) have $\log(R)$ values under 3.3, with one exception that comes in at 3.9. None of these regions exhibited a flare at M5 or higher. In contrast, all active regions with >M5 flares have values of $\log(R)$ exceeding 4.0 (see Table 2), and all have an increasing value of $\log(R)$ or are within 0.1 of that peak at the time of the major flaring; all but two have decreasing values of $\log(R)$ on average

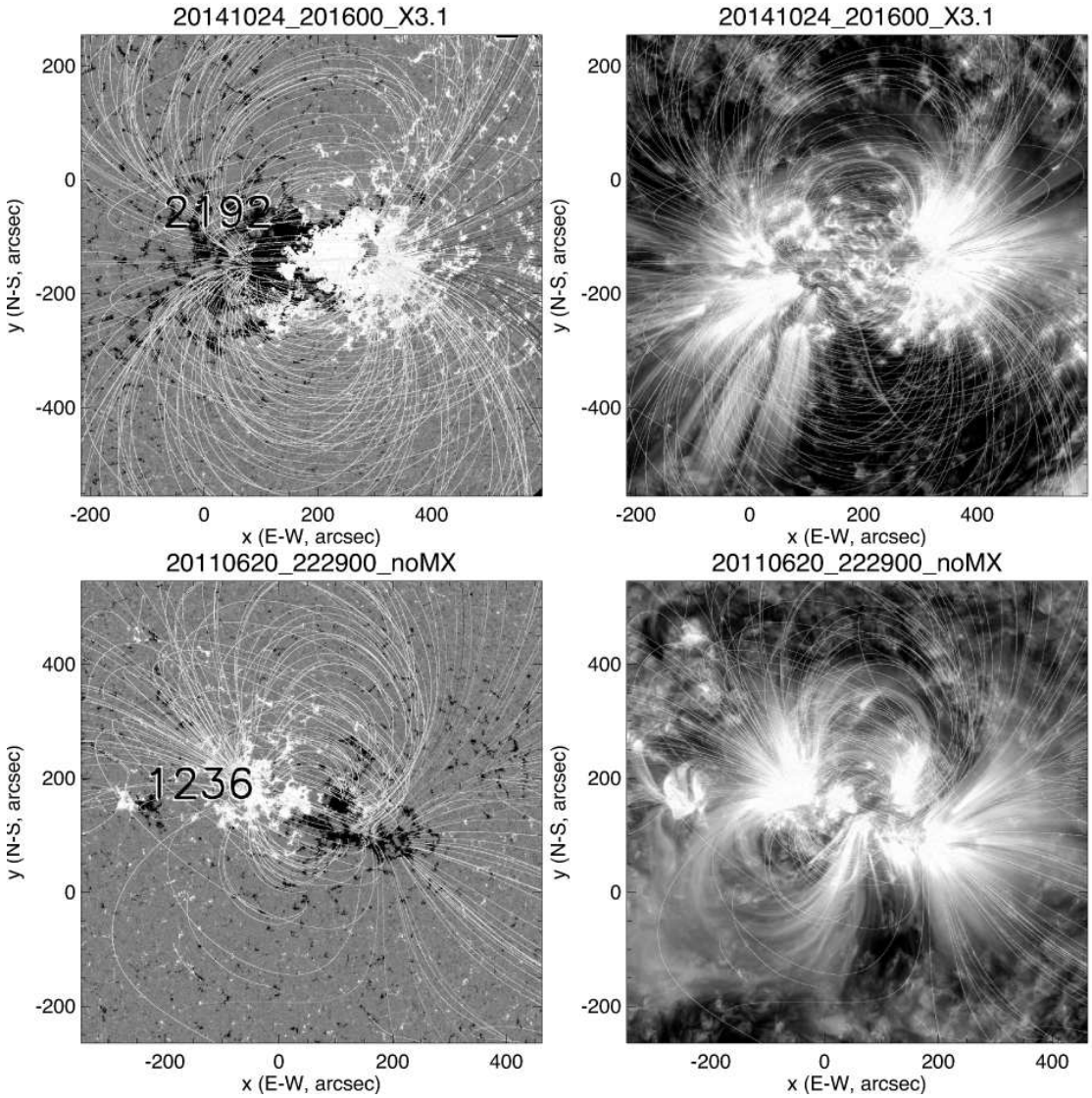

Figure 6. As Fig. 1: Example regions in category 'd', with and without X flares: *(top)* AR 12192 *(bottom)* AR 11236.

over the subsequent two days (excepting only AR 11520 and - weakly - AR 12192 on 2014/10/24); compare Fig. 7 and Table 3. Regions with X-class flares have high-R-value interiors associated with flux emergence and displacement, but many of these do not show obvious signs of nonpotentiality in the "outer" 171 Å loops; one example is AR 11283 which shows possibly nonpotential loops only in the area north of the leading spot (here the 6-h, 1-degree PFSS spatiotemporal resolution may be a limiting factor in the analysis). Others (e.g., AR 11429) have substantial nonpotential signatures in their outer loops and a high R-value interior (which, for this region, persists on subsequent days without M- or X-class flaring); this is also the case for AR 11944.

Active regions with $log(R) \geq 4$ without large flares all exhibit activity within them or within their immediate vicinity: AR 11330 which was close to, and possibly connected to, substantial eruptions on the northern side; ARs 11555/-60/-61 (which exhibit frequent eruptions); ARs 11864/-5 (with several large eruptions); and AR 11895/-7 (with eruptions and jets on 2013/11/17-18).

Table 3
Contingency table for the average 4-day trend in $\log(R)$ ending in M- or X-class flaring or not. Only three cases were omitted from this table owing to erratic behavior in R, which was low in each of these. Trends are denoted as "rising" or "falling" if the change exceeded a factor of two in a linear fit, "flat" otherwise.

Trend in $R(t)$:	falling	flat	rising	falling after X flare
no M or X flare	36	19	2	-
M or X flare	1	6	10	13 of 15

Three of the ten regions exhibiting M- or X-class flares do not display obvious signs of nonpotentiality in their active region-scale loops (classified as type "c" and/or "d" in Table 1): AR 11166, AR 11283, and AR 11890 (shown in the top panels of Fig. 1). Nonpotentiality of AR 12192 (Fig. 6, top) is particularly obvious in loops from its trailing, southern area. The side-by-side comparison in Fig. 8 suggests that a relatively long SHIL with shearing motions along it is important for a pronounced nonpotential appearance of active region-scale

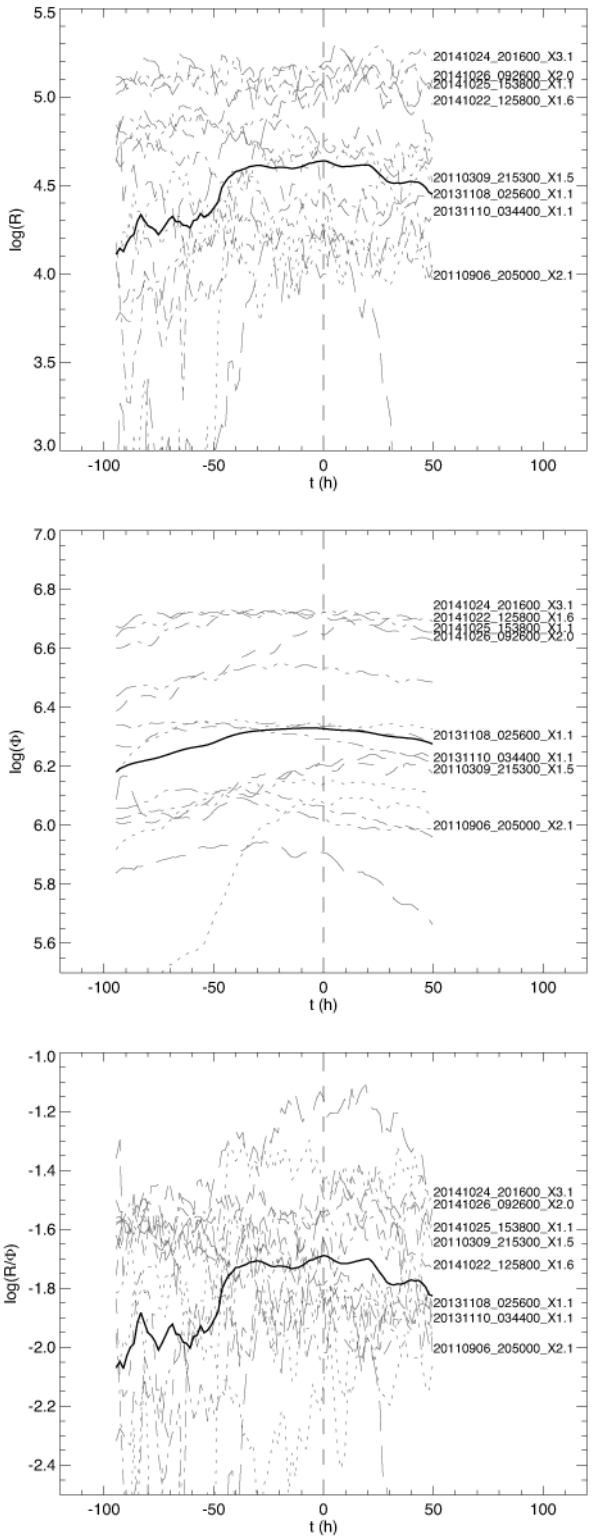

Figure 7. For regions with X-class flares, the superposed epoch diagrams show the values with time (on a 96-min. cadence) of $\log(R)$ (top), total absolute flux $log(\Phi)$ (in the same units of 2.2×10^{16} Mx, see Schrijver [2007] for rationale; center), and the fraction of the total absolute flux involved in the strong-field high-gradient inversion line $\log(R/\Phi)$ (SHIL; bottom). The curves have been shifted to the flare time as reference, and are shown in grey using various line styles; labels identify regions in class c or d. The heavy curve is the average superposed-epoch trend for the set of 15 X-class flares, shown after a 5-point boxcar smoothing.

loops. Work by Dalmasse *et al.* (2015) showed that such shearing motions involving the PIL induce non-neutralized currents in the surrounding corona, thereby contributing to the nonpotential appearance.

The three regions with near-potential coronae shown in Fig. 8 have SHILS off the primary PIL. The primary SHIL for AR 11890 at which the X1.1 flares occur is quite short and is located at the outer periphery of the active region. These properties may limit the influence of its current system on the region-scale loops. For the other two regions, the field geometry suggests that oppositely-directed mostly-parallel currents should be induced, thus weakening any effects on active-region scale loops. Specifically:

The flare in AR 11166 is associated with various clusters of mixed parasitic polarity that are caught in flows that push the various concentrations towards and along each other (see top-left panel in Fig. 8). The most pronounced SHIL just prior to the X1.5 flare is formed by a thin ridge of positive polarity sandwiched between negative polarities. In such a configuration, the velocity shear on the opposite sides of the positive-polarity ridge would be expected to induce oppositely-directed currents that would have largely canceling effects on the surrounding distant field. A comparable configuration and dynamics were described by Wang *et al.* (2014), who showed the oppositely-directed magnetic twist in a non-linear force-free field model for AR 11515 (their Fig. 2c, with a map of vertical currents in their Fig. 7i). In the X1.5 flare studied here, a second branch of the flaring area comprised a less pronounced, smaller, comparable configuration with negative polarity sandwiched between positive polarities (see Vemareddy and Wiegelmann (2014) for a discussion and NLFFF modeling of this event).

The X1.8 flare in AR 11283 is associated with a positive-polarity spot and surroundings being pushed into two negative-polarity patches on opposite sides, both containing spots with partly absent penumbrae (see, e.g., Fig. 2 in Ruan *et al.* 2015). As for the X1.5 flare in AR 11166, one can argue that oppositely-directed shear-induced current systems form between the three flux clusters.

Returning to the non-potential regions, Fig. 8 suggests that the length and location of the SHIL relative to the bulk of the region are important to nonpotentiality of the corona, but the magnitude of R will also play a role. The values of R for the selected regions show too little range to confirm this observationally. Moreover, as shown in Fig. 7 (bottom panel), the fraction of the flux involved in the SHILs for the largely potential X-flaring regions shows a spread comparable to the sample of all X-flaring regions, i.e., somewhere between 1% and 6% of the total absolute flux (note that the R metric involves only a fraction of the flux that is involved in flux emergence as it was quantified by Schrijver *et al.* 2005).

I note that the X-class flare from AR 11944, although in a region with sunspots, does not involve a region with a SHIL. This is the only flare in this study not directly overlying at least in part a high-R area. This is discussed somewhat more in the next section.

Over the period of this study, *SDO/AIA* observed all active regions on the disk, 1139 in total. Within the longitude selection window for this study of about 80°, some of these will not yet have emerged, while others will

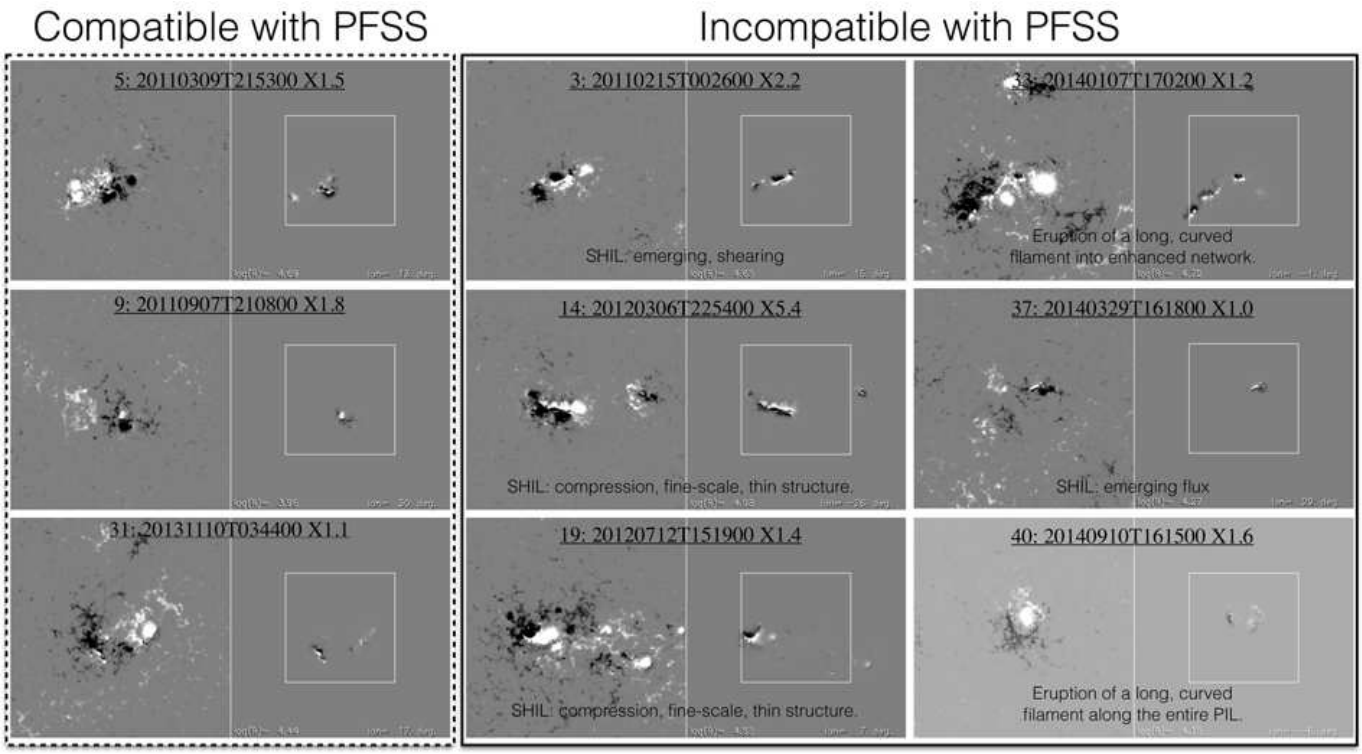
Compatible with PFSS
Incompatible with PFSS
5: 20110309T215300 X1.5
3: 20110215T002600 X2.2
SHIL: emerging, shearing
33: 20140107T170200 X1.2
Eruption of a long, curved filament into enhanced network.
9: 20110907T210800 X1.8
14: 20120306T225400 X5.4
SHIL: compression, fine-scale, thin structure.
37: 20140329T161800 X1.0
SHIL: emerging flux
31: 20131110T034400 X1.1
19: 20120712T151900 X1.4
SHIL: compression, fine-scale, thin structure.
40: 20140910T161500 X1.6
Eruption of a long, curved filament along the entire PIL.

Figure 8. Comparison of *HMI* magnetograms and corresponding R maps for regions with X-class flares; white lines encompass the 320-arcsec square areas within which R is measured. Regions with largely potential coronae are shown on the left in the dashed box; others on the right in the solid box. AR 12158 in which the X flare was not associated with a SHIL but with a long filament is shown in light gray. AR 12192, with regionally pronounced nonpotentiality, is excluded.

have their spots (and with it their NOAA number) disappear prior to entering the selection window. Assuming a characteristic active-region life time of order ten days, regions visible in the selection window will have emerged up to about 6 days before entering the selection window, or ≈80° behind the East limb. Regions can be given numbers to close to the West limb, so the total longitude range for numbered regions is ≈ 250°. The fraction of NOAA regions selectable here is thus ≈210/250, or somewhat over 80% of the total.

Of these ≈950 regions, only 37 were selected as substantially incompatible with the PFSS field, 5 of which may have their coronal configuration still distorted while relaxing from eruptions that occurred hours before the times of study, with another two regions being unnumbered bipolar regions. Consequently, only some $P_{\rm N}$ ≈3-4% of the sampled active regions appears nonpotential, at least within the roughly 5-day window during which such regions meet the selection criteria used here. Although the sampling is in principle unbiased as I reviewed all *AIA* data within about 40° of disk center, the subjective selection criterion used means this fraction should be interpreted with care. The sampling by Schrijver *et al.* (2005), in contrast, in which roughly equal numbers of the *TRACE* active-region pointings showed near-potential and nonpotential coronae, was similarly subjective but heavily biased by the pointing selections, often guided by community members interested in AR activity. The value of $P_{\rm N}$ lies well below the upper limit estimated for the fraction of "less than 30%" of the lifetime of active regions during which flaring is statistically observed (Schrijver *et al.* 2005).

In some of the nonpotential regions, no significant flux emerges during at least the 4 days preceding the time of the analysis (although there are the usual moving magnetic features in the moats of remaining sunspots, if any). These include all the regions with essentially zero R values: five numbered regions (ARs 11084, 11092, the region leading 11240, 11399, the essentially isolated spot region 11599), and the two unnumbered, spotless target regions Nos. 4 and 29. All have filaments in or next to them - signatures of current systems - but then so do most sample regions; Schrijver *et al.* (2005) found no differentiating filament characteristics between potential and nonpotential regions.

Schrijver *et al.* (2005) noted that they could not attribute the nonpotentiality to recent or ongoing flux emergence in 3 of 21 regions. Here, I find that 5 in 41 have had no flux emergence in at least the four days preceding the selected time, which is statistically un-differentiable from the number of nonpotential emergence-free regions in Schrijver *et al.* (2005). Apparently, nonpotentiality occurs for regions without (recent) flux emergence in some 10%-15% of cases; the two nonpotential spotless regions suggest nonpotentiality can exist even if the spotless region is dispersing into the network.

4. DISCUSSION AND CONCLUSIONS

This study uses 4.5 years of *SDO* observations to provide insight into the origin and role of electrical currents in active-region coronae. As part of this work, I look into how to integrate the conclusions from (a) Schrijver *et al.* (2005) who showed that regions with a distinctly nonpotential appearance of their coronae were - as an ensemble - twice as likely to flare, with average flare energies three times higher than for regions with largely potential

coronal fields, and (b) from Schrijver (2007) that large flares require substantial amounts of flux in strong-field, high-gradient polarity inversion lines (SHILs; expressed in a measure denoted R). With this study, the sample of nonpotential regions studied by Schrijver *et al.* (2005) is increased from 36 to 77, while the selection of the regions is free from the researcher-interest bias that guided the *TRACE* target selections.

Schrijver (2007) and Welsch and Li (2008) infer that, statistically speaking, the most common driver of the formation of the SHIL is flux emergence. That is confirmed by the present sample, although AR 11158 and possibly AR 11166 appear to be examples in which the SHILs form by shearing coalescence of previously emerged structures.

SHILs are transient, surviving typically for 1-2 days. This was noted in studies of relatively small samples (including Pevtsov *et al.* 1994; Schrijver *et al.* 2005; Aschwanden *et al.* 2014). Mason and Hoeksema (2010) performed a large-sample analysis of magnetograms of flaring regions using *SOHO/MDI* magnetograms, reviewing data for 1075 active regions and for 6000 C, M, and X flares. They find that "[f]lare occurrence is statistically associated with changes in several characteristics of the line-of-sight magnetic field in solar active regions (ARs). ... The best-calculated parameter, the gradient-weighted inversion-line length (GWILL), combines the primary polarity inversion line (PIL) length and the gradient across it. Therefore, GWILL is sensitive to complex field structures via the length of the PIL and shearing via the gradient. GWILL shows an average 35% increase during the 40 hr prior to X-class flares, a 16% increase before M-class flares, and 17% increase prior to B-C-class flares," followed by a decrease after the flare when analyzing behavior in a superposed epoch analysis. The present sample of regions shows consistent average trends (see Sect. 3 and Fig. 7). Based only on that, one might conclude in a statistical sense that the flux emergence at the SHIL completes within about a day of the flare time. The range in behavior for individual regions is so large, however, that this tendency for flux in the region and the SHIL to peak around the time of major flaring is not useful as a predictive indicator of either major flaring or termination of flux emergence for individual regions.

A case of particular interest here is that of AR 11944: whereas this region has a high value of $\log(R) = 4.7$ that frequently accompanies X-class flaring, the flare in fact stems from a filament eruption in a PIL that has no high-gradient field in it (but with the filament-carrying flux rope an obvious candidate contributor to the nonpotential appearance of the coronal field).

It is interesting in this context to note that there are very few known cases of flares of X magnitude that occur without involving a SHIL, or in regions in which no SHIL exists at al. Moore and Labonte (1980) and Svestka *et al.* (1982) describe a filament eruption from an old spotless region. Moore and Labonte (1980) show a BBSO videomagnetogram suggesting no SHIL, while the Hα filtergrams (e.g. Martin 1979) show a pronounced filament configuration running along the north-south oriented PIL. As this event occurred prior to the GOES satellites, whether or not it was indeed an X-class flare needs to be established indirectly; Svestka *et al.* (1982) discuss the X-ray observations of this event, yielding an emission measure of some $10^{50}\,\mathrm{cm}^{-3}$ and a temperature of ≈ 8.5 MK at peak emission measure (after cooling from a peak value of 10.4 MK), not atypical for an X flares.

What is the origin of largely un-neutralized currents that may lead to AR-scale nonpotentiality? Modeling work by Dalmasse *et al.* (2015) and others cited in Sect. 1 suggests that this requires shearing of the neutral line, such as is often seen accompanying flux emergence. The emergence of flux into pre-existing configurations can result in high-R SHILs. In the case of intense flaring, this occurs most frequently when the emerging flux bundle appears to be a current-carrying rope (which typically takes $1 - 2$ d to fully emerge), sometimes when emerging concentrations are pushed into and along pre-existing clusters of substantial flux (on time scales of hours to days), while rarely the currents survive or grow as the active region evolves and SHIL signatures vanish or even until spots have dissolved (which can take over a week).

Current systems leading to nonpotential configurations can also occur by rotation of flux concentrations, e.g., rotating sunspots (which would cause swirls in the loops above these, as is seen in at least 18 of the 37 substantively nonpotential regions in the sample). The work by Dalmasse *et al.* (2015) demonstrates that if such rotating motions are well away from the PIL, then direct and return currents should neutralize; yet, when these rotating motions involve much of the flux, the corona is likely still distorted relative to a potential configuration even if the current should neutralize overall.

Such bulk rotation of large flux clusters might be caused by subsurface vortices. Searching for relationships between surface field and subsurface flows, however, Seligman *et al.* (2014) "find no significant region-by-region correlation between the subsurface kinetic helicity and either the strong-field current helicity or α" (the ratio of current density and field strength in a nonlinear force-free field). In fact, "subsurface fluid motions with a given sign of kinetic helicity appear to correspond to photospheric field structures of the same and of opposite handedness in approximately equal numbers."

Signatures of electrical currents and of shearing (sometimes rotational) flows are seen as important for flaring behavior of active regions. Bobra and Couvidat (2015), for example, analyze 1.5 million observations of 2071 active regions in search for predictors of flaring activity. They identify four parameters as key discriminants for flaring: the total unsigned current helicity, total magnitude of the Lorentz force, total photospheric magnetic free energy density, and the total unsigned vertical current. All of these metrics can be derived only from vector-magnetic data. However, there are correlations that may point to comparably informative quantities that do not involve vector data. For example, Su *et al.* (2014), based on 3226 vector magnetograms of 61 active regions, show that total vertical absolute photospheric current and total unsigned flux in active regions are proportional over two orders of magnitude. Their sample includes regions that show no flaring of class C or above up to regions with X-class flaring. The Spearman rank correlation coefficient of that relationship is 0.98 and spread about the mean relationship is no wider than about a factor of 1.5 along the full range in fluxes (their Fig. 7b).

Net currents can apparently exist in some active regions (and in smaller spotless bipolar regions) well past the flux-emergence phase; perhaps, they can even be

Table 4
Contingency table for nonpotentiality and ≥X1 flaring in active regions between 2010/05/01 and 2014/10/31 estimated to meet the selection criteria for this study (see Sect. 3). The χ^2_ν test for independence of flaring and nonpotentiality yields $\chi^2_\nu = 115$.

No. of regions:	near-potential	nonpotential	total
no flares ≤M9	≈ 950	26	≈ 976
flaring at X1 or above	3	6	9
total	≈ 953	32	≈ 985

strengthened by sustained shear flows or by changes induced by the evolution of neighboring field, such as the emergence of an adjacent active region. Hence, old, decaying regions, some even past their spot-sporting phase (if ever they had spots), can appear nonpotential, often with filament eruptions from within them of from their interfaces with other (emerging, mature, or decayed) regions in the vicinity. This inference about sustained currents is to replace the hypothesis by Schrijver *et al.* (2005) who estimated the characteristic life time of current systems large enough to make the coronal field appear nonpotential to be of order 20-30 hrs upon termination of flux emergence, but did so based on a strongly biased selection of *TRACE* target regions.

The observations show all X-class flares to emanate from regions harboring SHILs, although 3 of 10 of these regions are not obviously nonpotential in a substantial part of their coronal appearance, and in one case the flare was not obviously connected to the SHIL. On the other hand, large regions can appear nonpotential without exhibiting major flaring. I conclude that the dynamics of the flux involved in the compact SHILs (which sets the regions' R values) is of preeminent importance for the large-flare potential of active regions, but that their corresponding currents may not reveal themselves in region-scale nonpotentiality, although their distorting field signatures are often seen low over the SHILs. The sample of X-flaring regions available to us, admittedly small, is consistent with MHD studies that suggest that their flux emergence off the main PIL may shield the effects of the currents involved through neutralizing counter-currents nearby. In contrast to the SHILs as diagnostic for flare potential, active region-scale nonpotentiality may inform us about the eruption potential other than those from SHILs, which almost never leads to X-class flaring.

The observations suggest that the electrical currents attending the nonpotential appearance of active-region coronae and those accompanying major flaring are significantly correlated (see the contingency Table 4), but not necessarily the same. Intense flaring generally occurs when flux is emerging, particularly when there are signatures of strong shearing flow and twisted field. Coronal nonpotentiality may result from sub-surface motions before the region emerges, as well as reflect ropes that intrude into the region later on, thus compounding successive generations of electrical currents through emergence and induction. Nonpotentiality generally occurs only in regions in which flux emergence is sufficiently large relative to existing flux (some 15% or more) and with strong-field high-gradient polarity inversion lines that are relatively long compared to the region's size scale and straddle the region's primary polarity inversion line. Nonpotentiality outlasts the flux-emergence and flaring phase of the regions' evolution by typically a day, but infrequently (in about 1 in 200 regions) it can last for over the four days of the sampling window used here.

I thank Mark Cheung and Alan Title for their comments, and Hugh Hudson for pointing out the "spotless" X flare of 1973. This work was supported by NASA's SDO/AIA contract (NNG04EA00C) to LMATC. *AIA* is an instrument onboard the *Solar Dynamics Observatory*, a mission for NASA's Living With a Star program.

REFERENCES

Aschwanden, M. J., Xu, Y., & Jing, J. 2014, ApJ. 797, 50
Barnes, G. & Leka, K. D. 2008, ApJL 688, 107
Bobra, M. G. & Couvidat, S. 2015, ApJ. 798, 135
Chen, H., Zhang, J., Ma, S., Yang, S., Li, L., Huang, X., & Xiao, J. 2015, ApJL 808, L24
Chifu, I., Inhester, B., & Wiegelmann, T. 2015, A&A 577, A123
Chintzoglou, G., Patsourakos, S., & Vourlidas, A. 2015, ApJ. 809, 34
Chintzoglou, G. & Zhang, J. 2013, ApJL 764, L3
Dalmasse, K., Aulanier, G., Démoulin, P., Kliem, B., Török, T., & Pariat, E. 2015, ApJ. 810, 17
DeRosa, M. L., Wheatland, M. S., Leka, K. D., Barnes, G., Amari, T., Canou, A., Gilchrist, S. A., Thalmann, J. K., Valori, G., Wiegelmann, T., Schrijver, C. J., Malanushenko, A., Sun, X., & Régnier, S. 2015, ApJ. 811, 107
Fang, F., Manchester, IV, W., Abbett, W. P., & van der Holst, B. 2012, ApJ. 754, 15
Handy, B. N., Acton, L. W., Kankelborg, C. C., Wolfson, C. J., Akin, D. J., Bruner, M. E., Carvalho, R., Catura, R. C., Chevalier, R., Duncan, D. W., Edwards, C. G., Feinstein, C. N., Freeland, S. L., Friedlander, F. M., Hoffman, C. H., Hurlburt, N. E., Jurcevich, B. K., Katz, N. L., Kelly, G. A., Lemen, J. R., Levay, M., Lindgren, R. W., Mathur, D. P., Meyer, S. B., Morrison, S. J., Morrison, M. D., Nightingale, R. W., Pope, T. P., Rehse, R. A., Schrijver, C. J., Shine, R. A., Shing, L., Strong, K. T., Tarbell, T. D., Title, A. M., Torgerson, D. D., Golub, L., Bookbinder, J. A., Caldwell, D., Cheimets, P. N., Davis, W. N., Deluca, E. E., McMullen, R. A., Amato, D., Fisher, R., Maldonado, H., & Parkinson, C. 1999, Solar Phys. 187, 229
Inoue, S., Hayashi, K., Magara, T., Choe, G. S., & Park, Y. D. 2015, ApJ. 803, 73
Janvier, M., Aulanier, G., Bommier, V., Schmieder, B., Démoulin, P., & Pariat, E. 2014, ApJ. 788, 60
Kazachenko, M. D., Fisher, G. H., Welsch, B. T., Liu, Y., & Sun, X. 2015, ApJ. 811, 16
Komm, R., Gosain, S., & Pevtsov, A. 2014, Solar Phys. 289, 475
Leibacher, J., Sakurai, T., Schrijver, C. J., & van Driel-Gesztelyi, L. 2010, Solar Phys. 263, 1
Leka, K. D. & Barnes, G. 2007, ApJ. 656, 1173
Lemen, J. R., Title, A. M., Akin, D. J., Boerner, P. F., Chou, C., Drake, J. F., Duncan, D. W., Edwards, C. G., Friedlaender, F. M., Heyman, G. F., Hurlburt, N. E., Katz, N. L., Kushner, G. D., Levay, M., Lindgren, R. W., Mathur, D. P., McFeaters, E. L., Mitchell, S., Rehse, R. A., Schrijver, C. J., Springer, L. A., Stern, R. A., Tarbell, T. D., Wuelser, J.-P., Wolfson, C. J., Yanari, C., Bookbinder, J. A., Cheimets, P. N., Caldwell, D., Deluca, E. E., Gates, R., Golub, L., Park, S., Podgorski, W. A., Bush, R. I., Scherrer, P. H., Gummin, M. A., Smith, P., Auker, G., Jerram, P., Pool, P., Soufli, R., Windt, D. L., Beardsley, S., Clapp, M., Lang, J., & Waltham, N. 2012, Solar Phys. 275, 17
Li, A. & Liu, Y. 2015, Solar Phys. 290, 2199
Liu, Y., Zhao, J., & Schuck, P. W. 2013, Solar Phys. 287, 279
Malanushenko, A., Schrijver, C. J., DeRosa, M. L., & Wheatland, M. S. 2014, ApJ. 783, 102
Malanushenko, A., Schrijver, C. J., DeRosa, M. L., Wheatland, M. S., & Gilchrist, S. A. 2012, ApJ. 756, 153
Manchester, W., Gombosi, T., DeZeeuw, D., & Fan, Y. 2004, ApJ. 610, 588

Martin, S. F. 1979, Solar Phys. 64, 165
Mason, J. P. & Hoeksema, J. T. 2010, ApJ. 723, 634
Metcalf, T. R., Derosa, M. L., Schrijver, C. J., Barnes, G., van Ballegooijen, A. A., Wiegelmann, T., Wheatland, M. S., Valori, G., & McTtiernan, J. M. 2008, Solar Phys. 247, 269
Moore, R. L. & Labonte, B. J. 1980, in M. Dryer and E. Tandberg-Hanssen (Eds.), *Solar and Interplanetary Dynamics*, Vol. 91 of *IAU Symposium*, p. 207
Pesnell, W. D., Thompson, B. J., & Chamberlin, P. C. 2012, Solar Phys. 275, 3
Petrie, G. J. D. 2012, ApJ. 759, 50
Petrie, G. J. D. 2013, Solar Phys. 287, 415
Pevtsov, A. A., Canfield, R. C., & Metcalf, T. R. 1994, ApJL 425, 117
Ruan, G., Chen, Y., & Wang, H. 2015, ApJ. 812, 120
Ruan, G., Chen, Y., Wang, S., Zhang, H., Li, G., Jing, J., Su, J., Li, X., Xu, H., Du, G., & Wang, H. 2014, ApJ. 784, 165
Savcheva, A. S., McKillop, S. C., McCauley, P. I., Hanson, E. M., & DeLuca, E. E. 2014, Solar Phys. 289, 3297
Scherrer, P. H., Bogart, R. S., Bush, R. I., Hoeksema, J. T., Kosovichev, A. G., Schou, J., Rosenberg, W., Springer, L., Tarbell, T. D., Title, A., Wolfson, C. J., Zayer, I., & The MDI Engineering Team 1995, Solar Phys. 162, 129
Scherrer, P. H., Schou, J., Bush, R. I., Kosovichev, A. G., Bogart, R. S., Hoeksema, J. T., Liu, Y., Duvall, T. L., Zhao, J., Title, A. M., Schrijver, C. J., Tarbell, T. D., & Tomczyk, S. 2012, Solar Phys. 275, 207
Schrijver, C. J. 2007, ApJL 655, 117
Schrijver, C. J. 2009, Advances in Space Research 43, 739
Schrijver, C. J., Aulanier, G., Title, A. M., Pariat, E., & Delannée, C. 2011, ApJ. 738, 167
Schrijver, C. J., De Rosa, M. L., Title, A.M., & Metcalf, T. R. 2005, ApJ. 628, 501
Schrijver, C. J. & DeRosa, M. L. 2003, Solar Phys. 212, 165
Schrijver, C. J. & Title, A. M. 2011, Journal of Geophysical Research (Space Physics) 116(A15), 4108
Schrijver, C. J., Title, A. M., Yeates, A. R., & DeRosa, M. L. 2013, ApJ. 773, 93
Seligman, D., Petrie, G. J. D., & Komm, R. 2014, ApJ. 795, 113
Su, J. T., Jing, J., Wang, S., Wiegelmann, T., & Wang, H. M. 2014, ApJ. 788, 150
Sun, X., Bobra, M. G., Hoeksema, J. T., Liu, Y., Li, Y., Shen, C., Couvidat, S., Norton, A. A., & Fisher, G. H. 2015, ApJL 804, L28
Sun, X., Hoeksema, J. T., Liu, Y., Wiegelmann, T., Hayashi, K., Chen, Q., & Thalmann, J. 2012, ApJ. 748, 77
Svestka, Z., Dodson-Prince, H. W., Mohler, O. C., Martin, S. F., Moore, R. L., Nolte, J. T., & Petrasso, R. D. 1982, Solar Phys. 78, 271
Toriumi, S., Iida, Y., Kusano, K., Bamba, Y., & Imada, S. 2014, Solar Phys. 289, 3351
Török, T. & Kliem, B. 2003, A&A 406, 1043
Török, T., Leake, J. E., Titov, V. S., Archontis, V., Mikić, Z., Linton, M. G., Dalmasse, K., Aulanier, G., & Kliem, B. 2014, ApJL 782, L10
Vemareddy, P., Ambastha, A., Maurya, R. A., & Chae, J. 2012, ApJ. 761, 86
Vemareddy, P. & Wiegelmann, T. 2014, ApJ. 792, 40
Wang, H. & Liu, C. 2015, Research in Astronomy and Astrophysics 15, 145
Wang, H., Liu, C., Deng, N., Zeng, Z., Xu, Y., Jing, J., & Cao, W. 2014, ApJL 781, L23
Wang, R., Yan, Y., & Tan, B. 2013, Solar Phys. 288, 507
Welsch, B. T. & Li, Y. 2008, in R. Howe, R. W. Komm, K. S. Balasubramaniam, and G. J. D. Petrie (Eds.), *Subsurface and Atmospheric Influences on Solar Activity*, Vol. 383 of *Astron. Soc. Pacific CS-*, 429